Applied Surface Science 370 (2016) 83–91

Contents lists available at ScienceDirect

Applied Surface Science

journal homepage: www.elsevier.com/locate/apsusc

Effect of substrate temperature on transparent conducting Al and F co-doped ZnO thin films prepared by rf magnetron sputtering

Fang-Hsing Wang*, Chiao-Lu Chang

Department of Electrical Engineering and Graduate Institute of Optoelectronic Engineering, National Chung-Hsing University, Taichung 40227, Taiwan, ROC

A R T I C L E I N F O

Article history:
Received 20 November 2015
Received in revised form 17 February 2016
Accepted 17 February 2016
Available online 21 February 2016

Keywords:
Al–F co-doped ZnO
Transparent conducting oxide (TCO)
Thin film
magnetron sputtering
Substrate temperature

A B S T R A C T

ZnO is a wide bandgap semiconductor that has many potential applications such as solar cells, thin film transistors, light emitting diodes, and gas/biological sensors. In this study, a composite ceramic ZnO target containing 1 wt% Al_2O_3 and 1.5 wt% ZnF_2 was prepared and used to deposit transparent conducting Al and F co-doped zinc oxide (AFZO) thin films on glass substrates by radio frequency magnetron sputtering. The effect of substrate temperatures ranging from room temperature (RT) to 200 °C on structural, morphological, electrical, chemical, and optical properties of the deposited thin films were investigated by X-ray diffraction (XRD), field emission scanning electron microscopy (FE-SEM), atomic force microscopy (AFM), Hall effect measurement, X-ray photoelectron spectroscopy, secondary ion mass spectrometry, and UV–vis spectrophotometer. The XRD results showed that all the AFZO thin films had a (0 0 2) diffraction peak, indicating a typical wurtzite structure with a preferential orientation of the *c*-axis perpendicular to the substrate. The FE-SEM and AFM analyses indicated that the crystallinity and grain size of the films were enhanced while the surface roughness decreased as the substrate temperature increased. Results of Hall effect measurement showed that Al and F co-doping decreased the resistivity more effectively than single-doping (either Al or F doping) in ZnO thin films. The resistivity of the AFZO thin films decreased from 5.48×10^{-4} to 2.88×10^{-4} Ω-cm as the substrate temperature increased from RT to 200 °C due to the increased carrier concentration and Hall mobility. The optical transmittances of all the AFZO thin films were over 92% in the wavelength range of 400–800 nm regardless of substrate temperature. The blue-shift of absorption edge accompanied the rise of the optical band gap, which conformed to the Burstein-Moss effect. The developed AFZO thin films are suitable as transparent conducting electrodes for various optoelectronic applications.

© 2016 Elsevier B.V. All rights reserved.

1. Introduction

Transparent conducting oxide (TCO) thin films are promising for applications in various optoelectronic devices, such as flat panel display, photovoltaic devices, light-emitting diodes, and waveguides [1–5]. Sn-doped In_2O_3 (ITO) films with relatively low resistivity in the order of 10^{-4}–10^{-5} Ω-cm are the most commonly used TCO films in optoelectronic devices. However, an increasing demand for scarce indium mineral causes an expensive material cost in the past decade. Zinc oxide (ZnO) has been recognized as promising substitute material of ITO in terms of its direct and wide band gap (3.37 eV), high abundance, low-price, non-toxicity and durability against hydrogen plasma in solar cell fabrication process [3,6]. The n-type conductivity of unintentionally doped ZnO films, attributing to intrinsic defects (such as oxygen vacancies and zinc interstitials) and/or others to noncontrollable hydrogen impurities introduced during growth [7–9], is still not enough high. Thus, various impurities have been used to dope into ZnO matrix to enhance the conductivity. ZnO thin films doped with group III elements such as B, Al, Ga, and In have been widely studied as TCO thin films due to superior optoelectronic properties and low material cost as well as non-toxicity [4–6,10–14]. Wang et al. have reported a resistivity of 2.39×10^{-3} Ω-cm in the 450 °C-annealed ZnO:B (BZO) films [5]. Kumar et al. have reported a resistivity as low as 4.89×10^{-4} Ω-cm along the carrier concentration 5.6×10^{20} cm^{-3} in their 200 nm-thick ZnO:Al (AZO) films [11]. Zhu et al. have reported that the resistivity of the ZnO:Ga (GZO) thin films ranges from 4.0×10^{-1} to 8.08×10^{-4} Ω-cm dependent on annealing temperature [12]. Previous literatures [3–14] indicated that the resistivity of the sputtered cation-doped ZnO thin films was in the order of 10^{-1} to 10^{-4} Ω-cm, which were higher than that of ITO ones [15]. Although it

* Corresponding author.
E-mail addresses: fansen@dragon.nchu.edu.tw, fansen920@gmail.com (F.-H. Wang).

http://dx.doi.org/10.1016/j.apsusc.2016.02.161
0169-4332/© 2016 Elsevier B.V. All rights reserved.

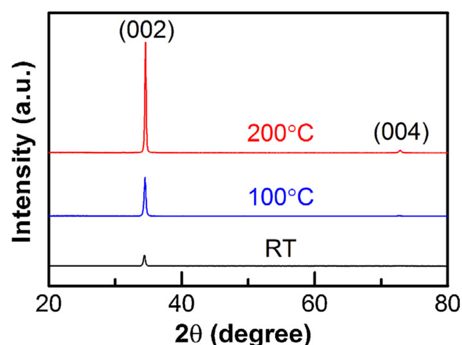

Fig. 1. XRD patterns and of AFZO thin films prepared at different substrate temperatures.

has been reported that resistivities as low as 8.5×10^{-5} Ω-cm and 8.1×10^{-5} Ω-cm were achieved for AZO [16] and GZO [17] thin films prepared by pulsed laser deposition. However, large-area deposition with high deposition rates is still challenging for pulsed laser deposition process.

Except these cation dopants, anion dopants such as F and Cl have been doped into ZnO films because they can substitute for oxygen in ZnO lattice to provide an extra conducting electron [18–26]. The ionic radius of F^- (131 pm) is close to that of O^{2-} (138 pm), and thus F is a suitable anion dopant to substitute O without introducing a large lattice distortion in ZnO crystal. A resistivity of 1.5×10^{-3} Ω-cm has been observed for the vacuum-annealed ZnO:F (FZO) thin films containing 2 at% F [18]. Our previous report showed a resistivity of 9.29×10^{-4} Ω-cm and an average visible transmittance of above 90% for sputtered FZO thin films with 1.5 wt% ZnF_2 in the sputtering target [19]. A theoretical understanding indicates that the substitution of oxygen by fluorine perturbs the valence band only, thereby leaving the conduction band relatively free from scattering, which could reduce light absorption and enhance carrier mobility [27]. Liang et al. [24] and Xu et al. [20] have reported the FZO thin films with considerably high Hall mobility of above 45 cm^2/V-s. However, the resistivity of the sputtered single dopant doped ZnO thin films is still inferior to that of the ITO thin film [18,19,26].

In the past decade, researches have used co-doping strategy to further improve the specific properties of ZnO thin films [28–42]. For example, group III element (Al, Ga, or In) and Mg co-doped ZnO thin films show a widened band gap and a good conductivity [28–30]. Al–Ni and Al–Co co-doped ZnO thin films have ferromagnetism [31,32]. Al and other group III element (B, Ga, or In) co-doped ZnO thin films exhibit lower resistivities than that of the AZO film [33–35]. Cation–anion co-doping of ZnO is less focused but worth exploring owing to the capability of tailoring electrical and optical properties of ZnO. N and a group III element (B, Al, or Ga) co-doped ZnO thin films have a p-type conductivity [36–38]. F and a group III or IV element (Al, Ga, or Sn) co-doped ZnO thin films have been studied [39–41]. Kim et al. [40] adopted two ceramic targets, i.e. ZnO:Al_2O_3 (3 wt%) and ZnO:ZnF_2 (0–10 wt%), to co-sputter Al and F doped ZnO (AFZO) thin films with varying fluorine content. Their results indicated that AZO thin films co-doped with a small amount of fluorine achieved a relatively low electrical resistivity of 5.9×10^{-4} Ω-cm. Shi et al. [41] developed high-quality Ga and F co-doped ZnO thin films by using mid-frequency sputtering and a low resistivity of 6.4×10^{-4} Ω-cm and a high visible transmittance of above 90% were obtained. Still there are not so many researches on this topic to clarify the detailed mechanism, especially co-dopants acting on the physical characteristics of ZnO thin films.

In this paper, a single ceramic ZnO target containing a small amount of Al_2O_3 and ZnF_2 was used to fabricate AFZO thin films by rf magnetron sputtering in pure Ar atmosphere at substrate temperatures (T_{sub}) of room temperature (RT), 100 °C, and 200 °C. The structural, morphological, electrical, chemical, and optical properties of AFZO thin films are investigated with various T_{sub}.

2. Experimental details

The composite ceramic target consists of 97.5 wt% ZnO (99.999%), 1.0 wt% aluminum oxide (Al_2O_3) (99.999%), and 1.5 wt% zinc fluoride (ZnF_2) (99.995%). First, these three types of the powders were mixed, dried and ground. Next, the mixed powders were pressed into a pellet using a steel die. After debindering, the pellet was calcined at 600 °C for 1 h and sintered at 1060 °C for 3 h to form a ceramic target with 2.5 in. in diameter and 5 mm in thickness.

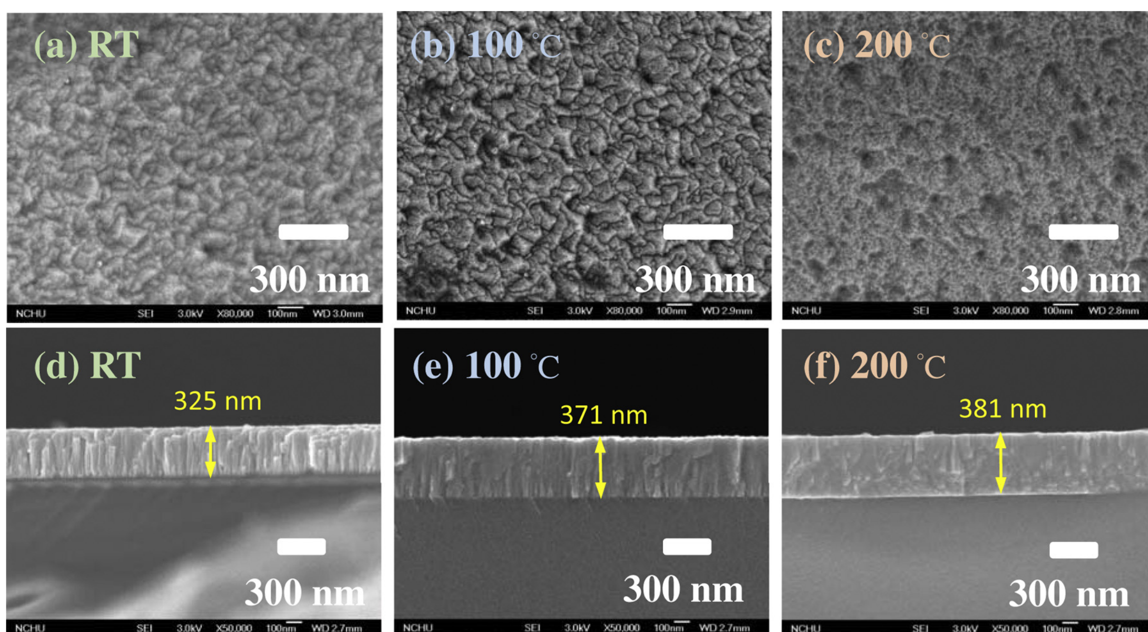

Fig. 2. FE-SEM photographs of AFZO thin films prepared at varying T_{sub}: plane-view: (a) RT, (b) 100 °C, and (c) 200 °C; cross-section view: (d) RT, (e) 100 °C, and (f) 200 °C.

Glass substrates (Corning Eagle XG) were cleaned subsequently in isopropyl alcohol (IPA) and deionized (DI) water, employing ultrasonic bath for 10 min in each step. Then, all samples were dried by flowing nitrogen gas. AFZO thin films of approximately 350 nm were deposited on glass substrates by rf magnetron sputtering at an rf power of 80 W (3.95 W/cm^2). The substrate temperature (T_{sub}), which was measured by a thermal couple attached on the substrate surface, ranged from RT (i.e. without intentional heating) to 200 °C because these temperatures were suitable for many industrial applications. The deposition rates of the AFZO thin films were 5.10, 5.51, and 5.65 nm/min at T_{sub} of RT, 100 °C, and 200 °C, respectively. The working distance from the target to the substrate holder is 8 cm. The base pressure in the chamber was below 6.67×10^{-4} Pa (5.0×10^{-6} Torr) and the working pressure was controlled at 0.667 Pa (5×10^{-3} Torr) in Ar ambient. During sputtering, the substrate holder was spun at 10 rpm to obtain better film uniformity.

The structure of the films was analyzed by X-ray diffraction (XRD, PANalytical) with Cu-Kα radiation (λ = 1.54056 Å, θ–2θ scan mode). The electrical properties were determined by Hall effect measurement (Ecopia, HMS-3000) using the Van der Pauw method with four pressed indium ball onto the corners of the sample under a 0.55 T magnetic field. The morphology of AFZO thin films was observed using field emission scanning electron microscopy (FE-SEM, JEOL, JSM–6700F) and atomic force microscopy (AFM, Digital Instrument, D5000) with a Nanoscope IV controller operated at tapping mode. The optical transmittance was measured by a UV–vis-NIR spectrophotometer (JASCO, V–570). X-ray photoelectron spectroscopy (XPS, ULVAC-PHI, 5000 Versaprobe) characterization was employed to analyze surface chemical composition and bonding after surface pre-cleaning for 3 min by sputtering. Secondary ion mass spectrometry (SIMS, Cameca, IMS-6f) was used to investigate fluorine contents within the samples. All the measurement and the analyses are performed at RT.

3. Results and discussion

3.1. Structural and morphological properties of AFZO thin films

Fig. 1 shows the θ–2θ scan XRD patterns of AFZO thin films with different T_{sub}. It was observed that a strong (0 0 2) diffraction peak appeared at the 2θ of around 34.5° due to its lowest surface free energy in this direction. It indicates that all the AFZO films have a wurtzite structure with a preferentially c-axis orientation. No Al_2O_3 or ZnF_2 phase was found in the XRD spectra. In addition, the peak intensity of the AFZO thin film increased with the increasing T_{sub}, indicating that the AFZO thin films prepared at the higher T_{sub} (200 °C) showed better crystalline quality than that deposited at the low T_{sub}. The enhancement of c-axis orientation with increasing T_{sub} is attributed to an advance in the surface diffusion of the adsorbed species. The similar results for ZnO [43], AZO [6,44], GZO [45,46], and FZO [47] thin films have also been observed. Table 1 lists the structural parameters of the AFZO thin films calculated from the XRD patterns. The crystalline plane distance (d) was determined from the Bragg diffraction equation: λ = 2dsinθ, where λ is the X-ray wavelength (1.54056 Å) and θ is the diffraction angle of the (0 0 2) peak. For hexagonal crystals with a highly c-axis preferred orientation, the film strain (ε) and stress (σ) can be quantitatively calculated based on biaxial strain model [48,49]. The strain (ε) in the films along the c-axis and the film stress (σ) parallel to the film surface are obtained by the following formulas:

$$\varepsilon = \frac{c_{film} - c_0}{c_0}, \quad (1)$$

$$\sigma = \frac{2c_{13}^2 - c_{33}(c_{11} + c_{12})}{2c_{13}} \times \varepsilon = -233 \times \varepsilon(\text{GPa}), \quad (2)$$

where c_{ij} is the elastic constant, c_{11} = 208.8 GPa, c_{33} = 213.8 GPa, c_{12} = 119.7 GPa, c_{13} = 104.2 GPa for single crystalline ZnO, c_{film} represents the lattice constant of c axis for the AFZO film and equals 2d, and c_0 = 0.5204 nm is the unstrained lattice parameter for ZnO powders [10,50]. The negative sign in Eq. (2) corresponds to compressive stress.

In AFZO thin films, Al (or F) is expected to substitute for Zn (or O) in its lattice site, thus shifting the 2θ value of the (0 0 2) peak from 34.0° of the ZnO film towards 34.40° of the AFZO film. The 2θ value further increased to 34.56° with increasing T_{sub} to 200 °C. Because the reduction in ionic radii of Al^{3+} (39 pm) substituting for Zn^{2+} (60 pm) is larger than that of F^- (131 pm) substituting for O^{2-} (138 pm), it is believed that 2θ shift is mainly attributed to Al^{3+} substituting for Zn^{2+} and F^- substituting for O^{2-} contributes a minor part [51,52]. This result agrees with our previous reports on AZO and FZO thin films [6,47], in which the right-shift of the (0 0 2) peak is larger for the AZO films than for the FZO films as the T_{sub} increased from RT to 200 °C. The substitutions of Al and F for Zn and O, respectively, also cause the reduction in crystalline plane distance, as Table 1 lists. The grain size is evaluated from the FWHM of the (0 0 2) peak using the Scherrer's formula [53]. The FWHM decreased accompanied the increase of grain size with the increasing T_{sub}. This result can be explained by that a high T_{sub} can enhance the crystallinity of films due to the rise of crystallization energy. The lattice parameter of c has been estimated to be in the range of 0.5198–0.5209 nm based on the XRD data. It was found that the T_{sub} also had great influence on film strain and stress. At the low T_{sub} (i.e. RT), a compressive stress (σ < 0) existed in the AFZO film, while it decreased and changed to a tensile stress (σ > the T_{sub} increased (≧100 °C). In general, the stress in the film consists of the thermal and intrinsic stress. The former is attributed to the different coefficient of thermal expansion (CTE) of film and substrate material; the latter originates from crystalline quality and defects across the films. The CTE of the Corning glass [54,55] is 3.17×10^{-6} K^{-1}, which is close to the CTE of ZnO (2.49×10^{-6} K^{-1} at 300 K and 4.26×10^{-6} K^{-1} at 700 K) [56,57]. Therefore, the thermal stress can be neglected in the present work and the only reason that dominates the film stress is intrinsic effect. At a low T_{sub}, the compressive stress is thought to be caused by the atomic peening effect of high-energy argon atoms and oxygen ions [58,59]. When T_{sub} rises, the adsorbed atoms possess more energy to form larger grain sizes; meanwhile, more Al and F atoms substitute for Zn and O atoms, respectively, at their lattice sites. Thus, the improved crystalline quality and the reduced number of defects release the compressive stress and result in the tensile stress. The similar phenomenon has been found by Zhu et al. [60] and Shi et al. [57].

Fig. 2 shows the plane-view and cross-section view FE-SEM images of AFZO thin films with T_{sub} from RT to 200 °C. It was found that the surface morphology of the films varied with T_{sub}. The films deposited at the low temperatures (RT–100 °C) were nanocrystalline with a porous surface, as indicated in Fig. 2(a) and (b), which exhibited a notable rough surface and might influence carriers moving on film surface, thus causing a low carrier mobility (see Fig. 4). The films exhibited a uniform columnar structures aligned with the c-axis orientation perpendicular to the substrate surface, but the column size was shrink as T_{sub} increased from RT to 100 °C, as shown in Fig. 2(d) and (e). This film structure is referred to zone I in Thornton structure zone model [61] on account of limited mobility of adatoms at a low T_{sub}. When T_{sub} went up to 200 °C, the films changed its surface morphology from rough to smooth and dense. The columnar grain growth was reduced and thus column boundaries of ZnO crystals became indistinct at T_{sub} of 200 °C, as shown in Fig. 2(c) and (f). It is attributed to that adsorbed species

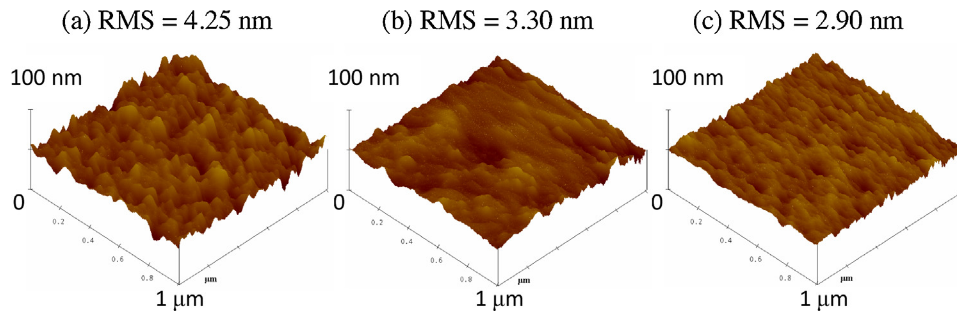

Fig. 3. AFM images of AFZO thin films prepared at different T_{sub}: (a) RT, (b) 100 °C, and (c) 200 °C.

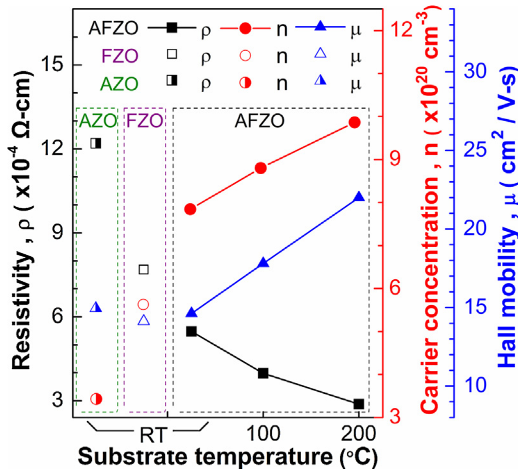

Fig. 4. Resistivity, Hall mobility, and carrier concentration of AFZO thin films as a function of T_{sub}.

receive enough energy to crystallize and form dense structure at the high T_{sub}. Besides, the thickness of all AFZO films was determined and approximately 350 ± 30 nm based on the cross-section images. The columnar structure of the AFZO thin films confirms the c-axis orientation growth as indicated by XRD patterns in Fig. 1.

The dependence of surface characteristics on T_{sub} was also investigated by AFM, as Fig. 3 shows. The images are obtained in tapping mode taken over a scale of 1 × 1 μm^2. The surface morphologies of the films were significantly affected by T_{sub} and their root mean square (RMS) roughness decreased from 4.25 to 2.90 nm as T_{sub} increased from RT to 200 °C. This result agrees with the analysis from FE-SEM. Previous reports also indicated that the surface roughness of the AZO and FZO thin films decreased as the substrate temperature increased from RT to 200 °C [43,47]. It is explained by that the oxygen ions in the plasma during the deposition process cause a re-sputtering effect, thus improving film roughness. However, oxygen is not externally introduced during our sputtering processes. According to FE-SEM results, column boundaries and rough surface were notablly observed with the AFZO films at the low T_{sub}. There should be many nucleation sites existing in the initial films and they have no enough energy to aggregate together for flatness of thin films. As T_{sub} rises towards high temperature such as 200 °C, the adatoms or adparticles will obtain enough energy to form a compact and flat film. Therefore, the crystal structure and surface roughness of the AFZO thin films are improved at the high T_{sub}.

3.2. Electrical properties and chemical composition of AFZO thin films

Fig. 4 shows the resistivity, Hall mobility and carrier concentration of AFZO thin films as a functional of T_{sub}. AZO and FZO thin films were also prepared for comparison under the same deposition conditions as the AFZO ones except using different sputtering targets. The targets for preparing AZO and FZO thin films contained 1.0 wt% Al_2O_3 and 1.5 wt% ZnF_2, respectively. The relationship between the carrier concentration, Hall mobility and resistivity can be described by the following equation:

$$\rho = \frac{1}{qn\mu}, \tag{3}$$

where ρ is resistivity, μ is Hall mobility, n is carrier concentration, and q is the electron charge. At T_{sub} of RT, it was observed that the resistivity was apparently lower for the AFZO thin film than for the AZO and FZO ones. It is worth noting that the low resistivity of the AFZO thin film results from the increase of carrier concentration because the differences in Hall mobility among the three types of the samples are relatively small. This result indicates that dual doping of Al and F benefits the free carrier concentration of ZnO thin films more than single dopant-doped films (i.e. either AZO or FZO thin films). Table 3 shows a comparison of the obtained electrical properties between n-type AZO, FZO and co-doped ZnO thin films prepared by magnetron sputtering. Except dopant type and amount, it is noted that the electrical properties of doped ZnO films are also dependent on deposition conditions (e.g. power density, chamber pressure, working distance, and sample position) and contaminations. For the AZO thin films, Minami et al. have reported the lowest resistivity of 1.9 × 10^{-4} Ω-cm [3]. However, most literatures showed a resistivity larger than 4 × 10^{-4} Ω-cm [4,6,11]. For the FZO thin films, it can be seen that the external substrate heating may decrease the resistivity as the sputtering uses the ZnO:ZnF_2 target [47]. For the co-doped ZnO thin films, the best results seem to arise from using an elevated substrate temperature and/or a high temperature annealing process because high temperature process improves the co-doping efficiency and crystalline quality within the films.

Furthermore, when T_{sub} increased from RT to 200 °C, the resistivity of the AFZO thin films decreased by a factor of two to one-half

Table 1
Structural parameters of AFZO thin films prepared at different substrate temperatures.

T_{sub} (°C)	2θ (°)	FWHM (°)	Grain size (nm)	d (nm)	c (nm)	Strain (×10^{-3})	Stress (GPa)
RT	34.40	0.338	24.60	0.2604	0.5209	1.06	−0.248
100	34.48	0.308	26.97	0.2599	0.5198	−1.19	0.277
200	34.56	0.239	34.74	0.2593	0.5186	−3.43	0.799

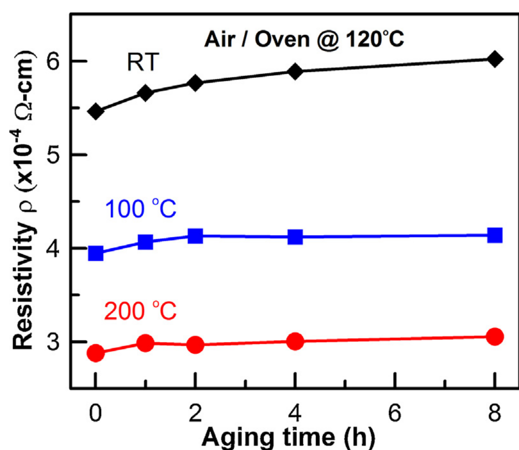

Fig. 5. Variation in resistivity of AFZO thin films prepared at varying T_{sub} as a function of aging time.

Table 2
XPS surface atomic ratios of AFZO thin films prepared at the T_{sub} of RT and 200 °C.

$T_{sub.}$	Zn 2p (at%)	O 1s (at%)	Al 2p (at%)	F 1s (at%)	C 1s (at%)
RT	36.6	42.7	1.1	<0.1	19.6
200 °C	52.6	42.6	1.2	<0.1	3.6

its original value, which accompanied by increases in both the Hall mobility and the carrier concentration. The enhanced Hall mobility with the increasing T_{sub} is attributed to the improved film crystallinity and the smooth film surface (see Figs. 1–3). The increased carrier concentration may be due to the enhanced doping efficiency and the reduced defects in the film. The optimal resistivity, Hall mobility, and carrier concentration are 2.88×10^{-4} Ω-cm, 22.0 cm^2/V-s, and 9.86×10^{20} cm^{-3}, respectively. The phenomenon that the resistivity of TCO films decreases with the increase of substrate temperature has been reported for AZO [6,44], GZO [45,46], and FZO [47] thin films.

Stability of the resistivity of AFZO thin films was measured by aging samples at 120 °C in an oven for 8 h in air atmosphere. Fig. 5 shows variation in the resistivity of AFZO thin films as a function of aging time. Results showed that the resistivities of all the films gradually increased during exposure to the 120 °C-air ambient. The lower T_{sub}, the larger increment of the resistivity was. It is attributed to that the films deposited at a lower T_{sub} has more defects on the surface and grain boundaries, which may adsorb oxygen species to obstruct carrier transport [62].

An XPS study was performed to investigate the chemical states of elements in AFZO thin films for clarifying the mechanism of the improvement in resistivity. Fig. 6 shows XPS spectra and their Gaussian-resolved components of O 1s, Zn $2p_{3/2}$, and Al $2p_{3/2}$ for the AFZO films prepared at the T_{sub} of RT and 200 °C. Qualitative analysis of XPS spectra (see Fig. 6a) indicated the presence of Zn, O, and C while Al and F peaks were not obvious due to relatively low contents in the films. The peak at around 284–285 eV is corresponding to C 1s and can be used to calibrate binding energies to compensate for surface charges effects [63]. Peaks at 1022, 140, 89, and 11 eV are attributed to Zn 2p, Zn 3s, Zn 3p, and Zn 3d, respectively. Zn LMM at 499 eV is the auger electron peak of Zn ion. A peak at around 531 eV corresponds to O 1s. Al 2p and F 1s peaks should be located at around 74.8 and 685.1 eV, respectively [64]. Table 2 lists XPS surface atomic ratios of AFZO thin films prepared at RT and 200 °C. The Al content was about 1.1%–1.2%, while the detected F content was less than 0.1% in the films. The detected relatively high C content for the RT-deposited sample is probably related to carbon contamination from CF_4 gas, which has ever been

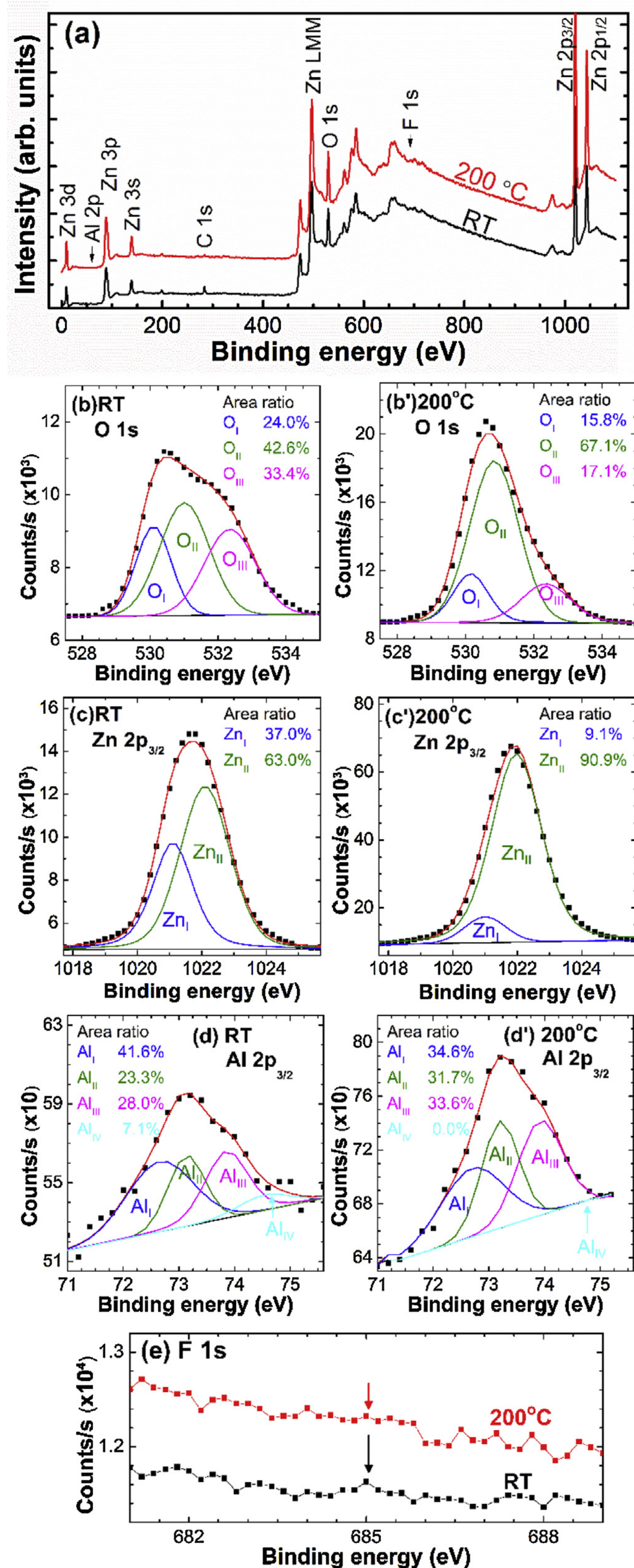

Fig. 6. (a) Overall XPS spectra and their Gaussian-resolved components of (b, b′) O 1s, (c, c′) Zn $2p_{3/2}$, (d, d′) Al $2p_{3/2}$, and (e) F 1s for the AFZO films prepared at the T_{sub} of RT and 200 °C.

Table 3
Electrical properties of n-type AZO, FZO and co-doped ZnO thin films prepared by magnetron sputtering.

Material	Resistivity (Ω-cm)	Carrier concentration (cm^{-3})	Hallmobility (cm^2/V-s)	Reference
ZnO:Al_2O_3 (2 wt%)	1.9×10^{-4}	1.5×10^{21}	22.0	[3]
ZnO: Al_2O_3 (2 wt%)	4.39×10^{-4}	6.96×10^{20}	20.46	[4]
ZnO: Al_2O_3 (2 wt%)	4.89×10^{-4}	5.6×10^{20}	22.8	[11]
ZnO: Al_2O_3 (1 wt%)	1.22×10^{-3}	3.43×10^{20}	14.95	This work
ZnO:CF_4 (0.4 vol%)	2.4×10^{-3}	1.53×10^{20}	17	[18]
ZnO:CF_4 (0.4 vol%, 150 °C-deposited)	4.4×10^{-3}	6.2×10^{19}	21	[18]
ZnO:ZnF_2 (1.5 wt%)	9.29×10^{-4}	3.86×10^{20}	17.4	[19]
ZnO: ZnF_2 (1.5 wt%)	7.69×10^{-4}	5.63×10^{20}	14.13	This work
ZnO:ZnF_2 (1.5 wt%, 300 °C-deposited)	5.27×10^{-4}	5.0×10^{20}	23.7	[47]
ZnO:Ga(2 at%)-Mg(5 at%)	6.89×10^{-4}	5.23×10^{20}	9.91	[30]
ZnO:Al-B (2 wt% each)	3.7×10^{-2}	7.1×10^{19}	2.4	[35]
ZnO:Al-B (2 wt% each, 600 °C-RTP)	7.9×10^{-4}	9.1×10^{20}	8.6	[35]
ZnO:Al-Ga (2 wt% each)	5.4×10^{-2}	9.9×10^{19}	1.2	[35]
ZnO:Al-Ga (2 wt% each, 600 °C-RTP)	4.4×10^{-4}	1.2×10^{21}	11.8	[35]
ZnO:Al_2O_3 (3 wt%)+ ZnO:ZnF_2 (1.3 wt%)	5.9×10^{-4}	5.15×10^{20}	20	[40]
ZnO:Ga_2O_3 (3 wt%)-ZnF_2 (2 wt%)	6.7×10^{-4}	6.8×10^{20}	13.4	[41]
ZnO:Al_2O_3 (1 wt%)-ZnF_2 (1.5 wt%) (RT-deposited)	5.48×10^{-4}	7.85×10^{20}	14.6	This work
ZnO:Al_2O_3 (1 wt%)-ZnF_2 (1.5 wt%)(200 °C-deposited)	2.88×10^{-4}	9.86×10^{20}	22	This work

used in the sputtering chamber, and carbon atoms adsorb on the film during exposure to the ambient atmosphere. When T_{sub} rises to 200 °C, some carbon atoms in the sputtering chamber may form volatilizable materials (CO*x* or CF*x*), which are easily pumped out of the chamber, thus decreasing the carbon content in the AFZO films. The bonding states of O 1s spectra are resolved into three peaks centered at 530.1 ± 0.1 (O_I), 531.2 ± 0.2 (O_{II}) and 532.4 ± 0.2 eV (O_{III}), respectively [65], as Fig. 6(b) and (b′) show. The O_I peak is owing to Zn—O bonds. The O_{II} peak is associated with $O_2{}^-$ ions in oxygen-deficient regions within the ZnO matrix. The O_{III} peak is usually attributed to chemisorbed or dissociated oxygen or OH species on the film surface [65]. As T_{sub} increased from RT to 200 °C, both the area ratios of the O_I and O_{III} peaks decreased while the area ratio of the O_{II} peak increased. It is well known that oxygen vacancies can create free electrons, while chemisorbed oxygen or OH species can capture free electrons. This result causes the increased free carriers at the high T_{sub}, as shown in Fig. 4. Fig. 6(c) and (c′) show narrow-scan spectra in the Zn $2p_{3/2}$ region and two resolved components for the AFZO thin films prepared at RT and 200 °C, respectively. The low binding energy component (Zn_I) centered at 1021.1 ± 0.1 is attributed to the presence of metallic Zn [6]. The high binding energy component (Zn_{II}) centered at 1022.1 ± 0.1 is due to Zn in the oxidized state (Zn—O) [65]. It was found that the decreased Zn_I area ratio accompanied with the increased Zn_{II} area ratio as the T_{sub} increased up to 200 °C, indicating that most of metallic Zn atoms were bound to oxygen for improving the crystallinity of the AFZO films. This finding consists with the result of the XRD analysis (see Fig. 1). Fig. 6(d) and (d′) show narrow-scan spectra in the Al $2p_{3/2}$ region and the resolved components for the AFZO thin films deposited at RT and 200 °C, respectively. The Al $2p_{3/2}$ peak is split into four components at 72.65 ± 0.1 eV (Al_I), 73.1 ± 0.1 eV (Al_{II}), 73.75 ± 0.1 eV (Al_{III}), and 74.7 ± 0.1 eV (Al_{IV}). The Al_I, Al_{II}, Al_{III}, and Al_{IV} components are attributed to the presence of metallic Al, Al_2O, AlO, and Al_2O_3, respectively [65–67]. As the T_{sub} rose from RT to 200 °C, reductions in the area ratios of the Al_I and Al_{IV} components accompanied with the increases of area ratios of the Al_{II} and Al_{III} ones. It reveals that high substrate temperature enhances the effectiveness of Al doping in the AFZO films, thus increasing free electrons in the films. Fig. 6(e) shows narrow-scan spectra in the F 1s region of the AFZO thin films deposited at RT and 200 °C. There seemed to be no obvious signal at around 685.1 eV, the binding energy of the F 1s peak, for both the AFZO films. This is due to the resolution limit of the equipment and the fact that some of F atoms probably do not form chemical bonds in ZnO lattices. However, it is believable that F exists in the prepared films and some of them may react chemically with the other elements owing to the improvement in the electrical properties of the AFZO and FZO thin films. It has been reported that the incorporation of F in the ZnO films may be a substitute for O as a donor to increase carrier concentration and may passivate dangling bonds at the surface and at grain boundaries to enhance carrier mobility [20,21]. To demonstrate existence of F in the developed AFZO thin films, the SIMS measurement was carried out. Fig. 7 shows the SIMS profiles of F within the as-deposited AFZO and ZnO thin films. It was found that the secondary F ion concentration was much higher (one order of magnitude or more) in the AFZO thin films than in the ZnO one. Based on the SIMS and XRD results, which prove the present of F and F^- can substitute for O^{2-} in the AFZO films, one can partly explain the improvement in their electrical properties. The above-mentioned results explain that the better carrier concentration and electrical conductivity of the AFZO film prepared at the higher T_{sub} is due to better Al doping effectiveness, F doping/passivation effect, less chemisorbed oxygen or OH species on the film surface, and more oxygen vacancies.

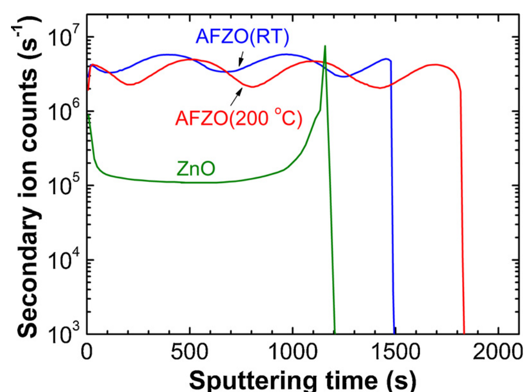

Fig. 7. SIMS profiles of fluorine within the AFZO and ZnO thin films.

3.3. Optical properties of AFZO thin films

Fig. 8(a) shows the optical transmittance spectra of AFZO thin films prepared at various T_{sub} as a function of incident light wavelength in 200–1500 nm. The observed difference in interference patterns indicated non-uniform thicknesses among the films (see Fig. 2). It was found that all the AFZO thin films exhibited superior visible transparencies and their average transmittance values in the wavelength interval of 400–800 nm were 92.37%, 92.85%, and 92.83% for the film deposited at RT, 100 °C, and 200 °C, respec-

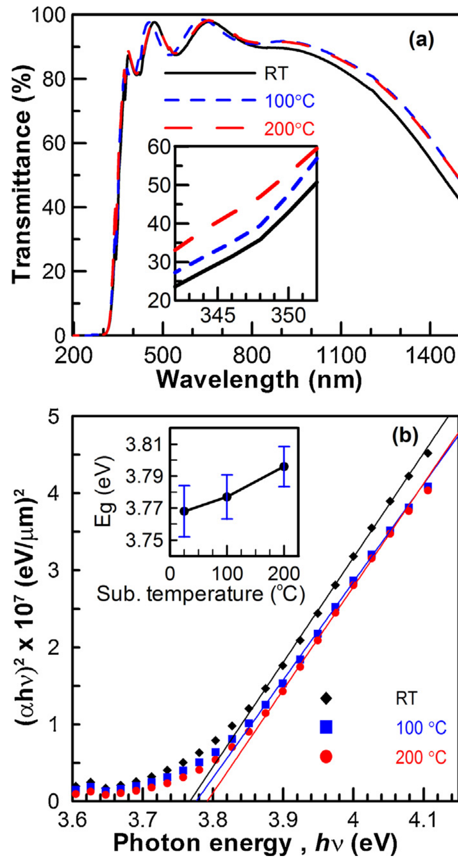

Fig. 8. (a) Optical transmittance spectra of AFZO thin films prepared at different T_{sub}. (b) Plot of $(\alpha h\upsilon)^2$ versus $h\upsilon$ near the band edge for AFZO films prepared at different T_{sub}. The solid lines represent the linear fit of the optical bandgap energy.

tively. It seems that the dependence of the visible transmittance of the AFZO thin films on substrate temperature is not significant. It is known that the optical transmission of doped ZnO thin films depends on film's thickness, morphology, and crystal structure, since the light absorption by a thicker film or light scattering induced by a rough surface and defects decreases the film's transparency. Though the film prepared at 200 °C possesses a better crystal quality and a smoother surface, however the thicker film than that prepared at RT may just counteract the advantage in transparency. Additionally, it is noted that the transmittance at the near infrared wavelength of 1200 nm exceeded 80%, revealing that the developed AFZO thin films are suitable as transparent electrodes for solar cell applications. Besides, all the transmittance spectra exhibited strong absorption edges in the UV region. The absorption edge shifted toward the short wavelength side with the increasing T_{sub}, as shown in the inset of Fig. 8(a). The similar results, the increased visible transmittance and the blue-shifted absorption edge, have also been observed in other TCO thin films [6,43,45,47]. The decreased transmittance in the near-infrared region is due to absorption of free carriers [68].

The optical band gap energy (E_g) of AFZO thin films can be estimated by Tauc plot [69,70], which uses an extrapolation method by dependence of optical absorption coefficient (α) on photon energy ($h\upsilon$) [22]:

$$\alpha h\upsilon = c(h\upsilon - E_g)^n \quad (4)$$

where c is the constant for direct transition, h is Planck's constant, υ is the frequency of the incident photon, and n is a constant ($n = 0.5$ is the allowed direct transition and $n = 2$ is the allowed indirect transition) [47]. In this study, the n value is set for 0.5 due to the

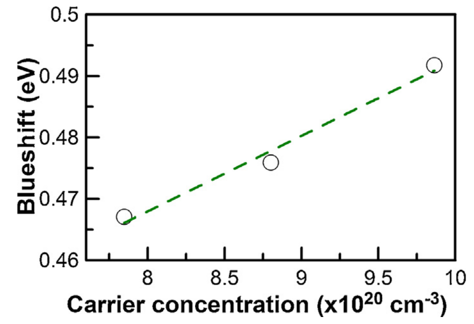

Fig. 9. Blue-shift of absorption edge of AFZO thin films as a function of carrier concentration.

direct transition type of the AFZO thin films. Fig. 8(b) shows the plot of $(\alpha h\upsilon)^2$ versus photon energy ($h\upsilon$) for the films prepared at various T_{sub} to determine E_g. The obtained E_g increased from 3.768 to 3.795 eV as T_{sub} rose from RT to 200 °C, as shown in the inset of Fig. 8(b). The variation in E_g, although very small, is indicative of the dependence of the optical band gap on the substrate temperature for the sputtered AFZO thin films. This result, the optical band gap broadening with the increasing T_{sub}, consists with the blue-shift of the absorption edge. This phenomenon was due to conduction band filling with electrons, known as the Burstein–Moss shift [71,72]. The effect occurs when the electron concentration exceeds a critical value and hence the electronic states surmount the bottom of the conduction band, causing that the electron transitions from the valence band to the conduction band require more energy than in the non-degenerate semiconductors. The optical band gap broadening is related to carrier concentration (n_e) in a degenerate semiconductor as the following equation [73]:

$$\Delta E_{BM} = \frac{h^2}{8m^*}\left(\frac{3}{\pi}\right)^{2/3} n_e{}^{2/3}, \quad (5)$$

where h is Planck's constant and m^* is the electron effective mass in the conduction band. The dependence of the observed blue-shift (ΔE_g) on n_e is shown in Fig. 9. Eq. (5) indicates that the band gap increases with the increasing carrier concentration. The relationship of the blue-shift (ΔE_{BM}) and the carrier concentration, as shown in Fig. 9, qualitatively demonstrated Eq. (5). To evaluate Eq. (5) quantitatively, set $m^* = 0.28 \times m_0$, where m_0 is the free electron mass. The calculated corresponding exponent of n_e in Eq. (5) is approximately 0.65, which is close to the theoretical value of 0.667 and conforms to the results of our previous investigation on AZO [6] and FZO [47] thin films (i.e., 0.64 for the AZO films and 0.69 for the FZO films).

4. Conclusions

Al and F co-doped ZnO thin films were deposited on glass substrates at RT, 100 °C, and 200 °C using a 1.5 wt% ZnF_2 and 1 wt% Al_2O_3 co-doped ZnO target by rf magnetron sputtering. All the AFZO thin films exhibited a typical wurtzite structure with a strong (0 0 2) preferred orientation regardless of substrate temperature. As the substrate temperature increased from RT to 200 °C, the grain size increased from 24.6 to 34.7 nm, the surface RMS roughness decreased from 4.25 to 2.90 nm, and the residual film stress changed from compressive to tensile type. The film resistivity significantly decreased by Al and F co-doping in comparison with single-dopant (either Al or F) doping in the ZnO films, revealing that the effectiveness of Al and F co-doping on electrical properties of ZnO thin films was higher than those of the Al or F-doped ZnO films. The electrical properties were also enhanced with the increase of substrate temperature and the lowest resistivity of the AFZO thin film was 2.88×10^{-4} Ω-cm at the substrate temperature of 200 °C,

accompanying by the carrier concentration of 9.86×10^{20} cm^{-3} and the Hall mobility of 22.0 cm^2/V-s. The mechanism of improvement in the electrical properties of the AFZO films has been presented. The XPS, XRD, and SIMS data revealed the enhancement of carrier concentration and conductivity is due to better Al doping effectiveness, F doping/passivation effect, less chemisorbed oxygen or OH species on the film surface, and more oxygen vacancies. The developed AFZO thin films had very high optical transmittances, that is, more than 92% in the visible range (λ = 400–800 nm) and more than 80% in the NIR region (λ = 1200 nm). The optical band gap was broadened from 3.767 to 3.791 eV with the increasing carrier concentration as the substrate temperature increased from RT to 200 °C, which conformed to the Burstein–Moss effect. The excellent electrical and optical properties reveal a great promise for the proposed AFZO thin films with applications in various optoelectronic devices.

Acknowledgement

The authors would like to thank Ministry of Science and Technology, Taiwan under the Grant MOST 103-2221-E-005-040-MY2 for financial support.

References

[1] D.S. Ginley, C. Bright, Transparent conducting oxides, MRS Bull. 25 (2000) 15–18.
[2] J. Hüpkes, B. Rech, O. Kluth, T. Repmann, B. Sehrbrock, J. Müller, R. Drese, M. Wuttig, Surface textured MF-sputtered ZnO films for microcrystalline silicon-based thin-film solar cells, Sol. Energy Mater. Sol. Cells 90 (2006) 3054–3060.
[3] T. Minami, Transparent conducting oxide semiconductors for transparent electrodes, Semicond. Sci. Technol. 20 (2005) S35–S44.
[4] Z.L. Tseng, P.C. Kao, C.S. Yang, Y.D. Juang, S.Y. Chu, Transparent Al-doped ZnO anodes in organic light-emitting diodes investigated using a hole-only device, Appl. Surf. Sci. 261 (2012) 360–363.
[5] Y. Wang, H. Huang, X. Meng, F. Yang, J. Nan, Q. Song, Q. Huang, Y. Zhao, X. Zhang, Electrical and structural properties of annealed ZnO:B thin films, J. Alloy. Compd. 636 (2015) 102–105.
[6] F.H. Wang, H.P. Chang, C.C. Tseng, C.C. Huang, Effects of H2 plasma treatment on properties of ZnO:Al thin films prepared by RF magnetron sputtering, Surf. Coat. Technol. 205 (2011) 5269–5277.
[7] Ü. Özgür, Y.I. Alivov, C. Liu, A. Teke, M.A. Reshchikov, S. Doğan, V. Avrutin, S.-J. Cho, H. Morkoç, A comprehensive review of ZnO materials and devices, J. Appl. Phys. 98 (2005) 041301.
[8] D.C. Look, J.W. Hemsky, J.R. Sizelove, Residual native shallow donor in ZnO, Phys. Rev. Lett. 82 (1999) 2552–2555.
[9] A. Janotti, C.G. Van de Walle, Hydrogen multicentre bonds, Nat. Mater. 6 (2007) 44–47.
[10] F.H. Wang, J.C. Chao, H.W. Liu, T.K. Kang, Physical properties of ZnO thin films codoped with titanium and hydrogen prepared by RF magnetron sputtering with different substrate temperatures, J. Nanomater. 2015 (2015), Article ID 936482, 11 pages.
[11] M. Kumar, L. Wen, B.B. Sahu, J.G. Han, Simultaneous enhancement of carrier mobility and concentration via tailor of Al-chemical states in Al-ZnO thin films, Appl. Phys. Lett. 106 (2015) 241903.
[12] D.L. Zhu, Q. Wang, S. Han, P.J. Cao, W.J. Liu, F. Jia, Y.X. Zeng, X.C. Ma, Y.M. Lu, Optimization of process parameters for the electrical properties in Ga-doped ZnO thin films prepared by r.f. magnetron sputtering, Appl. Surf. Sci. 298 (2014) 208–213.
[13] C.S. Tian, X.L. Chen, J.M. Liu, D.K. Zhang, C.C. Wei, Y. Zhao, X.D. Zhang, Wide-spectrum Mg and Ga co-doped ZnO–TCO thin films with introduced hydrogen grown by magnetron sputtering at room temperature, Appl. Surf. Sci. 314 (2014) 786–793.
[14] B.L. Wen, M. Kumar, B.B. Sahu, S.B. Jin, C. Sawangrat, K. Leksakul, J.G. Han, Advantage of dual-confined plasma over conventional and facing-target plasma for improving transparent-conductive properties in Al doped ZnO thin films, Surf. Coat. Technol. 284 (2015) 85–89.
[15] A. Suzuki, T. Matsushita, T. Aoki, Y. Yoneyama, Pulsed laser deposition of transparent conducting indium tin oxide films in magnetic field perpendicular to plume, Jpn. J. Appl. Phys. 40 (2001) L401–L403.
[16] H. Agura, A. Suzuki, T. Matsushita, T. Aoki, M. Okuda, Low resistivity transparent conducting Al-doped ZnO films prepared by pulsed laser deposition, Thin Solid Films 445 (2003) 263–267.
[17] S.M. Park, T. Ikegami, K. Ebihara, Effects of substrate temperature on the properties of Ga-doped ZnO by pulsed laser deposition, Thin Solid Films 513 (2006) 90–94.
[18] H.S. Yoon, K.S. Lee, T.S. Lee, B. Cheong, D.K. Choi, D.H. Kim, W.M. Kim, Properties of fluorine doped ZnO thin films deposited by magnetron sputtering, Sol. Energy Mater. Sol. Cells 92 (2008) 1366–1372.
[19] F.H. Wang, Y.H. Lee, T.K. Kang, H.W. Liu, Influence of RF power on physical properties of ZnO:ZnF2 thin films by RF magnetron sputtering, Superlattices Microstruct. 83 (2015) 289–298.
[20] H.Y. Xu, Y.C. Liu, R. Mu, C.L. Shao, Y.M. Lu, D.Z. Shen, X.W. Fan, F-doping effects on electrical and optical properties of ZnO nanocrystalline films, Appl. Phys. Lett. 86 (2005) 123107.
[21] Y.J. Choi, K.M. Kang, H.H. Park, Anion-controlled passivation effect of the atomic layer deposited ZnO films by F substitution to O-related defects on the electronic band structure for transparent contact layer of solar cell applications, Sol. Energy Mater. Sol. Cells 132 (2015) 403–409.
[22] Z. Pan, P. Zhang, X. Tian, G. Cheng, Y. Xie, H. Zhang, X. Zeng, C. Xiao, G. Hu, Z. Wei, Properties of fluorine and tin co-doped ZnO thin films deposited by sol–gel method, J. Alloy. Compd. 576 (2013) 31–37.
[23] E. Chikoidze, M. Nolan, M. Modreanu, V. Sallet, P. Galtier, Effect of chlorine doping on electrical and optical properties of ZnO thin films, Thin Solid Films 516 (2008) 8146–8149.
[24] H. Liang, R.G. Gordon, Atmospheric pressure chemical vapor deposition of transparent conducting films of fluorine doped zinc oxide and their application to amorphous silicon solar cells, J. Mater. Sci. 42 (2007) 6388–6399.
[25] D.L. Cao, L. Zhu, J. Jiang, R. Zhao, Z. Ye, B. Zhao, Highly transparent and conducting fluorine-doped ZnO thin films prepared by pulsed laser deposition, Sol. Energy Mater. Sol. Cells 95 (2011) 894–898.
[26] R.E. Treharne, K. Durose, Fluorine doped ZnO thin films by RF magnetron sputtering, Thin Solid Films 519 (2011) 7579–7582.
[27] R.G. Gordon, Criteria for choosing transparent conductors, MRS Bull. 25 (2000) 52–57.
[28] X.L. Chen, J.M. Liu, J. Ni, Y. Zhao, X.D. Zhang, Wide-spectrum Mg and Ga co-doped ZnO TCO thin films for solar cells grown via magnetron sputtering with H2 introduction, Appl. Surf. Sci. 328 (2015) 193–197.
[29] I.Y. Kim, S.W. Shin, M.G. Gang, S.H. Lee, K.V. Gurav, P.S. Patil, J.H. Yun, J.Y. Lee, J.H. Kim, Comparative study of quaternary Mg and group III element co-doped ZnO thin films with transparent conductive characteristics, Thin Solid Films 570 (2014) 321–325.
[30] S.W. Shin, G.L. Agawane, I.Y. Kim, S.H. Jo, M.S. Kim, G.S. Heo, J.H. Kim, J.Y. Lee, Development of transparent conductive Mg and Ga co-doped ZnO thin films: Effect of Mg concentration, Surf. Coat. Technol. 231 (2013) 364–369.
[31] M. Yu, H. Qiu, X. Chen, H. Li, W. Gong, Al and Ni co-doped ZnO films with room temperature ferromagnetism, low resistivity and high transparence, Mater. Chem. Phys. 126 (2011) 797–803.
[32] L.E. Mir, Z.B. Ayadi, M. Saadoun, K. Djessas, H.J. von Bardeleben, S. Alaya, Preparation and characterization of n-type conductive (Al, Co) co-doped ZnO thin films deposited by sputtering from aerogel nanopowders, Appl. Surf. Sci. 254 (2007) 570–573.
[33] J. Liu, W. Zhang, D. Song, Q. Ma, L. Zhang, H. Zhang, X. Ma, H. Song, Comparative study of the sintering process and thin film sputtering of AZO, GZO and AGZO ceramics targets, Ceram. Int. 40 (2014) 12905–12915.
[34] S.U. Park, J.H. Koh, Low temperature rf-sputtered In and Al co-doped ZnO thin films deposited on flexible PET substrate, Ceram. Int. 40 (2014) 10021–10025.
[35] C.A. Gupta, S. Mangal, U.P. Singh, Impact of rapid thermal annealing on structural, optical and electrical properties of DC sputtered doped and co-doped ZnO thin film, Appl. Surf. Sci. 288 (2014) 411–415.
[36] G.X. Liu, F.K. Shan, W.J. Lee, B.C. Shin, H.S. Kim, J.H. Kim, Boron and nitrogen co-doped ZnO thin films for opto-electronic applications, Ceram. Int. 34 (2008) 1011–1015.
[37] F. Zhu-Ge, Z.Z. Ye, L.P. Zhu, J.G. Lü, B.H. Zhao, J.Y. Huang, Z.H. Zhang, L. Wang, Z.G. Ji, Electrical and optical properties of Al–N co-doped p-type zinc oxide films, J. Cryst. Growth 268 (2004) 163–168.
[38] K. Shtereva, S. Flickyngerova, V. Tvarozek, I. Novotny, J. Kovac, A. Vincze, Characterization of gallium–nitrogen co-doped zinc oxide thin films prepared by RF diode sputtering, Vacuum 86 (2012) 652–656.
[39] A. Mallick, S. Sarkar, T. Ghosh, D. Basak, An insight into doping mechanism in Sn–F co-doped transparent conducting ZnO films by correlating structural, electrical and optical properties, J. Alloy. Compd. 646 (2015) 56–62.
[40] I. Kim, K.S. Lee, T.S. Lee, J.H. Jeong, B. Cheong, B.K. Cheong, Y.J. Baik, W.M. Kim, Effect of fluorine addition on transparent and conducting Al doped ZnO films, J. Appl. Phys. 100 (2006) 063701.
[41] Q. Shi, K. Zhou, M. Dai, S. Lin, H. Hou, C. Wei, F. Hua, Growth of high-quality Ga–F codoped ZnO thin films by mid-frequency sputtering, Ceram. Int. 40 (2014) 211–216.
[42] W. Lee, S. Shin, D.R. Jung, J. Kim, C. Nahm, T. Moon, B. Park, Investigation of electronic and optical properties in Al-Ga codoped ZnO thin films, Curr. Appl. Phys. 12 (2012) 628–631.
[43] X.Y. Li, H.J. Li, Z.J. Wang, H. Xia, Z.Y. Xiong, J.X. Wang, B.C. Yang, Effect of substrate temperature on the structural and optical properties of ZnO and Al-doped ZnO thin films prepared by dc magnetron sputtering, Opt. Commun. 282 (2009) 247–252.
[44] H.B. Zhou, H.Y. Zhang, M.L. Tan, Z.G. Wang, Effects of substrate temperature on the efficiency of hydrogen incorporation on the properties of Al-doped ZnO films, Superlattices Microstruct. 51 (2012) 644–650.
[45] F.H. Wang, H.T. Tzeng, C.C. Huang, Effects of deposition temperature on the properties of Ga-doped ZnO thin films, J. Sci. Innovation 4 (2014) 7–12.

[46] S.K. Kim, S.H. Kim, S.Y. Kim, J.H. Jeon, T.K. Gong, D.H. Choi, D.I. Son, D. Kim, Effect of substrate temperature on the structural electrical, and optical properties of GZO/ZnO films deposited by radio frequency magnetron sputtering, Ceram. Int. 40 (2014) 6673–6676.
[47] F.H. Wang, C.F. Yang, Y.H. Lee, Deposition of F-doped ZnO transparent thin films using ZnF2-doped ZnO target under different sputtering substrate temperatures, Nanoscale Res. Lett. 9 (2014) 97.
[48] R. Hong, J. Shao, H. He, Z. Fan, Influence of buffer layer thickness on the structure and optical properties of ZnO thin films, Appl. Surf. Sci. 252 (2006) 2888–2893.
[49] P. Mele, T. Endo, S. Arisawa, C. Li, T. Tsuchiya, Oxide Thin Films, Multilayers, and Nanocomposites, Springer International Publishing (ebook), Switzerland, 2015, pp. 243.
[50] H. Karzel, W. Potzel, M. Köfferlein, W. Schiessl, M. Steiner, U. Hiller, G.M. Kalvius, D.W. Mitchell, T.P. Das, P. Blaha, K. Schwarz, M.P. Pasternak, Lattice dynamics and hyperfine interactions in ZnO and ZnSe at high external pressures, Phys. Rev. B 53 (1996) 11425–11438.
[51] R.D. Shannon, Revised effective ionic radii and systematic studies of interatomic distances in halides and chalcogenides, Acta Crystallogr. Sect. A 32 (1976) 751–767.
[52] R. Dronskowski, Computational Chemistry of Solid State Materials, WILEY-VCH Verlag GmbH & Co KGaA, Weinheim, 2005, pp. 13–16.
[53] B.D. Cullity, S.R. Stock, Elements of X-ray Diffraction, 3rd ed., Prentice Hall, 2001, pp. 167.
[54] p. 1 http://www.howardglass.com/pdf/eagle_xg.pdf.
[55] C.F. Klingshirn, B.K. Meyer, A. Waag, A. Hoffmann, J. Geurts, Zinc Oxide: from Fundamental Properties towards Novel Applications, Springer-Verlag, Berlin Heidelberg, 2010, pp. 11.
[56] W. Water, S.Y. Chu, Physical and structural properties of ZnO sputtered films, Mater. Lett. 55 (2002) 67–72.
[57] Q. Shi, K. Zhou, M. Dai, H. Hou, S. Lin, C. Wei, F. Hu, Room temperature preparation of high performance AZO films by MF sputtering, Ceram. Int. 39 (2013) 1135–1141.
[58] J.A. Thornton, D.W. Hoffman, Stress-related effects in thin films, Thin Solid Films 171 (1989) 5–31.
[59] T. Sasabayashi, N. Ito, E. Nishimura, M. Kon, P.K. Song, K. Utsumi, A. Kaijo, Y. Shigesato, Comparative study on structure and internal stress in tin-doped indium oxide and indium-zinc oxide films deposited by r.f. magnetron sputtering, Thin Solid Films 445 (2003) 219–223.
[60] B.L. Zhu, S.J. Zhu, J. Wang, J. Wu, D.W. Zeng, C.S. Xie, Thickness effect on structure and properties of ZAO thin films by RF magnetron sputtering at different substrate temperatures, Phys. E 43 (2011) 1738–1745.
[61] D. Song, A.G. Aberle, J. Xia, Optimisation of ZnO:Al films by change of sputter gas pressure for solar cell application, Appl. Surf.Sci. 195 (2002) 291–296.
[62] B.Y. Oh, M.C. Jeong, J.M. Myoung, Stabilization in electrical characteristics of hydrogen-annealed ZnO:Al films, Appl. Surf. Sci. 253 (2007) 7157–7161.
[63] J.S. Bae, J.H. Yoon, S.K. Park, J.P. Kim, E.D. Jeong, M.S. Won, K.S. Shim, H.K. Yang, S.S. Yi, J.H. Jeong, Li-doping effect on the cathodoluminescent properties of Y2O3:Eu3+ phosphors, Surf. Rev. Lett. 14 (2007) 535–538.
[64] X. Noirfalise, T. Godfroid, G. Guisbiers, R. Snyders, Synthesis of fluorine doped zinc oxide by reactive magnetron sputtering, Acta. Mater. 59 (2011) 7521–7529.
[65] M. Chen, X. Wang, Y.H. Yu, Z.L. Pei, X.D. Bai, C. Sun, X-ray photoelectron spectroscopy and auger electron spectroscopy studies of Al-doped ZnO films, Appl. Surf. Sci. 158 (2000) 134–140.
[66] J.P. Kar, S. Kim, B. Shin, K.I. Park, K.J. Ahn, W. Lee, J.H. Cho, J.M. Myoung, Influence of sputtering pressure on morphological, mechanical and electrical properties of Al-doped ZnO films, Solid State Electron. 54 (2010) 1447–1450.
[67] K. Uma, M. Rusop, T. Soga, T. Jimbo, Effects of Al content on Zn0.95Mg0.05O thin films deposited by sol–gel spin coating, Jpn. J. Appl. Phys. 46 (2007) 40–44.
[68] R. Buonsanti, A. Llordes, S. Aloni, B.A. Helms, D.J. Milliron, Tunable infrared absorption and visible transparency of colloidal aluminum-doped zinc oxide nanocrystals, Nano Lett. 11 (2011) 4706–4710.
[69] J. Tauc, Optical properties and electronic structure of amorphous Ge and Si, Mater. Res. Bull. 3 (1968) 37–46.
[70] O. Stenzel, The Physics of Thin Film Optical Spectra: an Introduction, 2nd ed., Springer International Publishing, Switzerland, 2005, pp. 214.
[71] E. Burstein, Anomalous optical absorption limit in InSb, Phys. Rev. 93 (1954) 632–633.
[72] L.Y. Chen, W.H. Chen, J.J. Wang, F.C.N. Hong, Y.K. Su, Hydrogen-doped high conductivity ZnO films deposited by radio-frequency magnetron sputtering, Appl. Phys. Lett. 85 (2004) 5628–5630.
[73] T.S. Moss, The interpretation of the properties of indium antimonide, Proc. Phys. Soc. B 67 (1964) 775–782.